Experimental Mechanics (2012) 52:153–159
DOI 10.1007/s11340-011-9548-2

On the Failure and Dynamic Performance of Materials

N.K. Bourne

Received: 9 January 2011 / Accepted: 1 September 2011 / Published online: 25 October 2011

Abstract Waves induced by impact initiate deformation mechanisms within a material that precede later flow. An impulse excites a cascade of deformation mechanisms starting with ultrafast and concluding with slower ones. In metals, brittle glasses and polycrystalline ceramics there are a combination of mechanisms with differing relaxation times that condition a loaded target. In the case of ballistic impact, once failure has occurred, long rod penetration can occur and the depth achieved within each target can be scaled with the deformation strengths recorded during the initial high pressure impulse. A review of material shock response and target preconditioning shows a correlation with the ballistic penetration of the target after loading. This indicates that the effect of an initial loading impulse upon material behaviour is a strong feature of the effects observed in many dynamic phenomena.

Keywords Shock · Failure · Spall · Penetration · Akrology

Introduction

The dynamic response of materials and structures is determined by a range of mechanisms operating at the microstructural length scale [1, 2]. These are fixed by the boundary conditions applied by the load which the structure sees. The resulting response at the continuum is the integrated result of these operating mechanisms. For instance, if the stress rises rapidly above the relevant threshold (for instance within a shock), and the pulse lasts for sufficiently long that the mechanism completes before it is relieved, the material may change state and shows response relevant to the initial damage introduced by the shock.

Work has progressed with both metals and brittle materials and has determined, for a limited number within this set, a complete history of test data across a suite of impulses that gives an overview of the time evolution of the state of a material after compressive loading [3, 4]. The final observed properties of an impact-loaded material appear as an integration of these operating mechanisms with their different thresholds and timescales. In one-dimensional loading, only target recovery, developed to ensure precisely known continuum loading conditions, allows uniequivocal exploration of operating mechanisms [5]. These processes occur over a small time and a restricted volume but represent critical processes that condition the target for later deformation. In the case of ballistics for instance, the entry of a projectile and flow of fractured material around it at later times are a function of the nucleation phase which defines the boundary condition for subsequent inelastic flow within the material.

The deformation of a crystalline solid can be grouped into a series of deformation mechanisms with notional relaxation times in the following manner (Table 1). The first moments see the nucleation of dislocation cores at vacancy and local defect sites within the lattice. Shear of the unit cell of the material changes its phase to a denser polymorph. Such processes are fast in low defect density, crystalline solids and the kinetics of such changes are sub nanosecond [6]. Plasticity is evident in the first moments as twinning down suitable directions accommodating a proportion of the imposed strain on the target. Further flow occurs by slip which continues until dislocations become

N.K. Bourne (✉)
AWE,
Aldermaston,
Reading RG7 4PR, UK
e-mail: neil.bourne@mac.com

Table 1 Characteristic length and time scales for observing typical crystalline deformation mechanisms in a single-phase metal after applying step compression loading at t=0

Mechanism	Representative time scale	
Defect activation	100 ps	
Phase transformation	1 ns	Nucleation
Twinning	1 ns	
Slip	10 ns	Inelastic flow
Dislocation interaction	100 ns	
Pinning at boundaries	1 μs	
Void growth	1 μs	Equilibration and
Adiabatic shear	10 μs	Localisation
Surface morphology	100 μs	
Buckling	1 s	Mechanics
Creep	10 s	

immobile as a result of interactions with themselves or crystal boundaries. At longer times, new surfaces and materials of different impedance can create larger scale structures with longer characteristic timescales. Tensile damage can occur by void growth or localized shear across zones triggered at positions achieved at particular critically resolved shear stresses and boundary orientations. At longer timescales again, wave equilibration ensures a Newtonian response with application of the continuum precepts of mechanics. These groups of mechanisms can be grouped into four characteristic divisions characterized by indicative times. The Nucleation Phase; sub nanosecond, the Inelastic Flow Phase; sub microsecond; the Equilibration and Localization Phase; sub millisecond, and the Mechanics Phase in the realm greater than these times (see examples and order of magnitude process relaxation times in Table 1). In ballistic impact into semi-infinite targets the nucleation phase is defined by the shock loading phase within the first moments of impact which conditions the material for the following inelastic flow.

As loading time increases and each of these regimes is activated (integrating mechanisms from those operating previously), shear stress is relieved by the operating deformation mechanisms and the resulting measured strength lowers.

The regimes of Table 1 can be extended to substitute deformation mechanisms within brittle solids. The inhomogeneities within such a material cause local mesoscale damage to propagate, transiting from its elastic state and defining the onset of inelastic behaviour within it. It is possible to suppress failure in the continuum in a one dimensional experiment, since these global boundary conditions constrain the damage propagation. However, introducing a flaw into a material by design allows the propagation of the front to progress from a line source on the impact face and gives a measure of the initial value of the failed strength.

Establishing the Inelastic State

The first moments of impact ahead of a travelling impactor inevitably drive a shock into a solid. The material class will determine the failure mode and within each there will be a range of varying responses. A series of representative materials' properties are presented in Table 2. The key to representing the inelastic deformation of these materials is that the relevant mechanisms are activated to induce the inelastic state and have run to completion in the target material. Thus whilst the critical times are short the strains required in a test to produce an indicative failed strength are small.

A plate impact experiment delivers a well-defined pulse into a stationary target that allows tracking of the stress states as the pulse disperses. On the impact face, the pulse is square and as it progresses through the target it disperses with elastic wave travelling faster than the plastic at lower stresses with a step developing and an overdriven single front at higher stresses. The position of a stress sensor determines a Lagrangian station at which a continuum state variable is monitored. There is a uniaxial strain but a biaxial, cylindrically symmetric stress state in the target at the continuum but a fully three-dimensional state at inhomogeneities in the microstructure. The longitudinal stress may be measured with a suitably mounted sensor. Now the direct measurement of the lateral stress with piezoresistive gauges has been developed to allow use of the sensor in impact experiments. Gauges are mounted at a known distance from the impact face in a target reassembled from two tiles with a gauge mounted between. The geometrical arrangement for this is shown in Fig. 1. In some cases two gauges are mounted into the target to monitor the state developing at a particular stress level. Experiments are repeated to measure longitudinal stress histories at the same gauge location so that direct monitoring of all components of the stress history may be made. It should be pointed out from the outset, that embedded sensors are introduced into a flow and may perturb the stress state in which they are mounted. If their dimensions are small and their mounting is such that stress equilibrates quickly then they track the state around their location. However, to embed within a brittle target requires a cut in the sample into which they are inserted and this must also not affect the state that they monitor. All such gauges localize deformation in tension and fail the target so yield no information. But in the small strain, compressive loadings considered here, they can be shown to operate with precision and have been so calibrated so that one can rely upon the state parameters generated.

Table 2 Selected properties of the materials studied [7]

	ρ (±0.05 gcm^{-3})	E (GPa)	μ (GPa)	ν	c_L (±0.01 mm μs^{-1})	c_S (±0.01 mm μs^{-1})	HEL (±0.5 GPa)	2τ (±0.2 GPa)
4340	7.85	277	83	0.30	5.94	3.26	1.0	1.0
SL	2.49	73	30	0.23	5.84	3.46	4.0	1.9
AD85	3.42	221	91	0.22	8.81	5.24	6.1	5.3
AD995	3.89	436	151	0.23	10.66	6.28	6.7	5.5
B_4C	2.51	451	192	0.18	13.90	8.70	16.0	7.1
SiC	3.16	422	181	0.16	11.94	7.57	13.5	11.4
TiB_2	4.48	522	238	0.09	10.91	7.31	15.0[a]	13.0

[a] the upper

It is possible to suppress failure at the continuum in plate impact experiments on ceramics by symmetrical impact, so reducing lateral strains at the impact face. Using different impedance materials and a sectioned sample allows a failure zone to be propagated from the surface. This allows the determination of an upper bound for the initial value of the failed strength and in compression. Clearly tensile failure occurs at very much lower stresses in brittle materials. The behaviour followed here assumes failure under compression and correlation with ballistic penetration shows that it is compressive failure that dominates in this case. In multidimensional flow, the stresses are believed to be lower than the value in plate impact since there are more degrees of freedom of motion of the material.

The lateral stress, σ_y, and the longitudinal stress, σ_x, in a homogeneous, isotropic target measured at the length scale of the sensor sampling the flow, to calculate the shear strength τ of the material using

$$2\tau = \sigma_x - \sigma_y \tag{1}$$

This quantity has already been shown to be an indicator of the ballistic performance of materials in previous work [7–9]. This method of measuring shear strength is direct since no computation of the hydrostat is required. Additionally, its expected value can be calculated within the elastic range using the well-known relations

$$\sigma_y = \frac{\nu}{1-\nu}\sigma_x \text{ and thus } 2\tau = \frac{1-2\nu}{1-\nu}\sigma_x, \tag{2}$$

where ν is the Poisson's ratio.

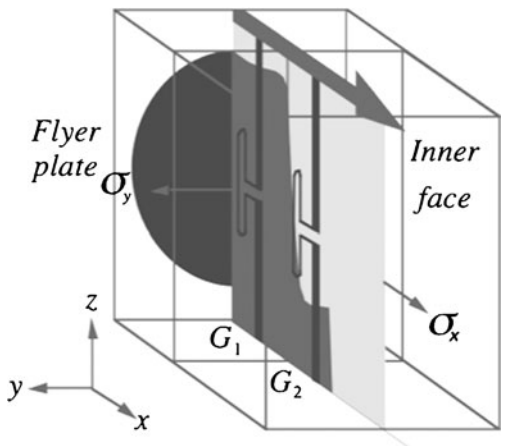

Fig. 1 Experimental arrangement used in experiments showing sectioning of target and insertion of gauges

Figure 2 shows the impulse recorded at a Lagrangian sensor for a BCC metal and a glass. The longitudinal and lateral stress components of the axisymmetic stress field at a Lagrangian gauge location are shown in dashed lines for each material. In the case of the BCC Ta shown, the longitudinal stress pulse shows that an elastic precursor has arrived before the plastic front rises to the Hugoniot stress at the gauge station [10]. The sensors are limited in their activation times with the first 200 ns of lateral stress not reliable since the wave is sweeping the gauge element and thus it is removed from these shear stress histories. The lateral stress rises to a peak behind the front after this time as it is swept by the wave. The solid curve shows twice the shear strength behind the pulse at ca. 4 GPa when the gauges are active, decaying after 1 μs to around 2 GPa. Lower values have been measured using ramp loading elsewhere [11]. This reduction occurs over a time interval which is an order of magnitude slower for a BCC material then is the case for an FCC one which indicates the speed of operating dislocation generation and storage mechanisms behind the shock for the two different crystal structures [12]. It is this defect activation and equilibration time which differentiates material classes and leads to differences in the observed dynamic response in continuum experiments.

Figure 2(b) shows longitudinal and lateral stress histories for a shot at a stress above the elastic limit of soda-lime glass. The stress traces for longitudinal and lateral stress rise in a ramped manner achieving a plateau after *ca.* 300 ns. The strength remains at its elastic value for the first 500 ns after which a drop occurs where twice the value goes from *ca*. 4 to 2 GPa. This corresponds with the arrival of a fracture front driven from the impact face of the glass and known as a failure wave [13–15]. This wave is a front

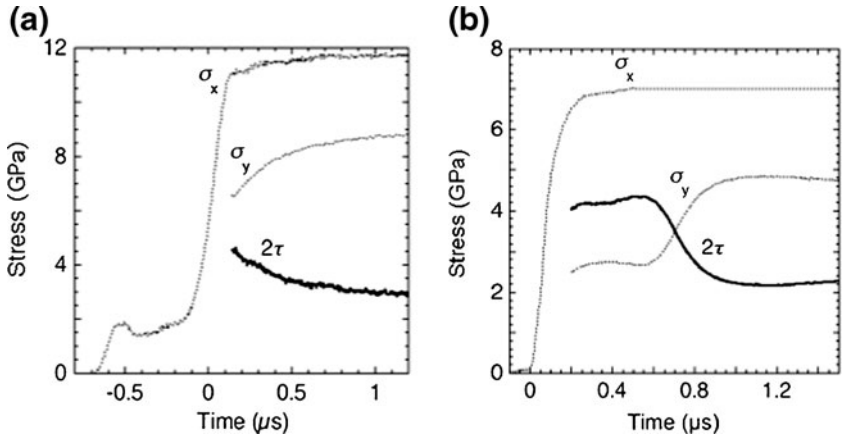

Fig. 2 Longitudinal and lateral stress histories for (**a**) BCC tantalum and (**b**) SL glass targets. The response in the elastic region where gauge equilibration occurs is not shown in the solid shear stress curves

across which there is a delayed transition to the inelastic state over a stress range up to 10 GPa. The metal and the glass are displaying the same behaviour consistent with their microstructural response to the step impact load. In the first moments both adopt an elastic state with corresponding elastic strength. Defects within the microstructure propagate from nucleation sites until they can interact and take the material to a plastic state. In the tantalum, the defects are dislocations that travel from the existing population in the metal. In a glass, the means of relieving the shear stresses is by crack nucleation and propagation at the Rayleigh wave speed in the material (90% of the shear wave speed in glass). These processes and defect densities mean that the elastic state starts to relax after ca. 100 ps in a metal whereas in glass that time is ca. 500 ns. At stresses above 10 GPa, the glass fails directly within the front to the steady state Hugoniot.

These times reflect two factors which control the strength. Defect density in the as-received microstructure and the mechanism of deformation that operates to define the inelastic state. Dislocation activation, transport and interaction in polycrystalline metals occurs three orders of magnitude faster than fracture that leads to comminution in amorphous glass. This illustrates how materials with limited ductility but equivalent hardness make better armour materials than metals by virtue of their slower failure kinetics. Further, these experiments define not only the kinetics but also the strengths of the materials as a function of pressure.

When the shock reaches a gauge station, material around it must initially respond in an elastic manner to the stimulus. Over some time processes will take place that allow the material to attain an inelastic state and these proceed reducing the shear stress in the material, by dislocation motion in metals and micro-fracture in brittle materials. The initial value of the lateral stress and the strength is given by the equations (2) which determines the initial state of the material. The kinetics of the processes leading to inelastic deformation determine the time taken to achieve the inelastic state. In the case of the glass, the initial strength for the shock (seen in Fig. 2(b)) is the elastic strength for the glass at a longitudinal stress of 7 GPa whereas the failed strength is 2.3 GPa which compares with 2.6 GPa derived using a simple Griffith's fracture criterion. Thus the glass retains its elastic strength for 0.5 μs until cracks interconnect and it fails to a fracture-controlled yield surface.

Figure 3 shows the response of the armour alumina, AD995 [17]. In Fig. 3(a), three wave profiles are shown taken from the work of Grady [16]. The histories show typical form for aluminas. There is a rapid rise to the first elastic limit, then a convex region to a point of inflexion and then a concave section rising (at the highest stress amplitudes) to the peak of the shock. It has been shown that the convex part of the pulse; from the first break from the elastic rise to the second point of inflexion on the rising pulse, corresponds to the mixed response region resulting from grain anisotropy [17]. The lower yield corresponds to slip in the basal plane and the upper to shock down the c-axis of the alumina grain which has no resolved stresses in this plane. In a polycrystalline target this means that an assemblage of elastically deformed grains exists within a matrix of plastically deformed grains favouring fracture at the weakly bound grain boundaries. Further twinning in the grains is favoured over slip and so fracture across grains down twin boundaries is also observed [18].

Figure 3(b) shows an experiment at the lower of these stress levels to ca. 10 GPa. The HEL of the ceramic, AD995 is 6.71 GPa [17]. The longitudinal and lateral stresses rise to the HEL quickly but then more slowly to the Hugoniot stress. Near to the impact face the stress remains high for around 500 ns before decaying to a lower value. Again, the material can display an elastic strength for some time before it returns to an inelastic state. The damaged material on the other hand has a failed strength of ca. 5 GPa at this stress level.

In each case (metal, glass and polycrystalline ceramic) the shock excites failure under the applied shear stress;

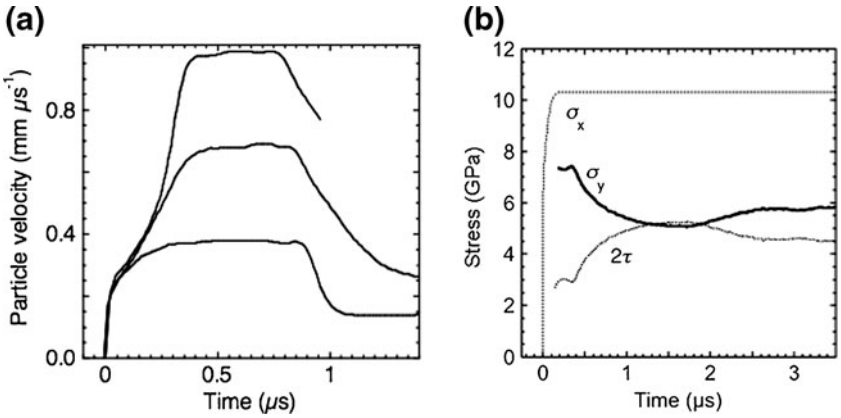

Fig. 3 (**a**) Longitudinal particle velocities for AD995 recorded from the work of Grady [16]. (**b**) Longitudinal and lateral stress histories (*dashed*) and shear stress history (*solid*) for AD995

dislocation motion in metals, fracture in glass, and fracture and twinning within grains with the ceramic. The material state has moved to the inelastic flow curve by the end of the pulse, but the time taken for that flow to be established is nanoseconds for the metal, hundreds of nanoseconds for the glass, and a microsecond for the ceramic. Up to this point, the material shows strength retained from its elastic value until the relaxation time of the process has been completed. It is at this time that penetration of a projectile may occur into a semi-infinite target.

Inelastic Flow

When a long, dense metal rod strikes a ceramic armour panel there are high transient stresses driven in behind shock fronts generated beneath its nose whilst the metal deforms on the surface. At later times slower rising waves are generated preconditioning the target. This impacted zone initiates damage that determines the resistance to the penetrator as it enters the armour. Surface effects known as dwell represent a conditioning environment for failure with its own failure kinetics. Inertial confinement defines a high-pressure environment that causes metallic armour to yield by plastic flow accompanied by processes such as shear banding, whereas penetration mechanisms in ceramics involve micro-fracture and fragmentation. The resistance experienced by a penetrating long rod is in the wake of failed material that is preconditioned in the impact zone by a propagating shock which initiates failure in the material. The shock itself is relieved by release from the edges of the rod after divergent flow is established in the target. The steady penetration phase is governed by flow through this medium with resistance supplied by the target material described analytically by the Alexeevski-Tate equation [19, 20]. In such cases the appropriate strength is that of the failed material mediated by the integrated effects of other operating mechanisms such as friction or shear. If the inelastic failure of the material controls the penetration then the time taken for the first transition to a failed state will be a critical step in the penetration. The failed strength measured in a well controlled experiment gives a maximum value for that seen in impact.

The processes that occur to fail a target do so in the first microsecond of shock loading in a target. If these mechanisms can be completed during the time that there is inertial confinement in the target, it is then possible to measure the inelastic strength of materials in an idealized loading geometry at an appropriate rate, and then apply the data derived to define the conditions operating during the impact event. An idealized experiment of choice has geometrically simple boundary conditions to allow material properties to be unequivocally defined. For the regime ahead of a penetrator, plate impact loading provides the correct range of conditions appropriate to the impact event considered even given that the mechanisms operating in metals and ceramics proceed at different timescales by dint of the restricted inelastic flow possible in brittle solids. Dislocation motion and twinning are operative on nanosecond timescales whereas the volume additive process, fracture, operates several orders of magnitude more slowly. This high resistance to flow directly determines the ballistic properties of an armour as illustrated below.

It follows that the failed strength, determined in plate impact in the manner described for alumina above, might correlate with the penetration of a rod in a depth of penetration (DoP) test. A series of such experiments has been conducted and results have been collated here to test this behaviour. This data is analysed here to assess the correlation between failed strength and DoP [21, 22]. Further, the failed strengths of a range of ceramics corresponding to these ballistic experiments have been conducted and are documented elsewhere [6]. Out of the large quantity of data presented in these, this work focuses on experiments conducted so that impact velocity was held constant and normal penetration into tiles of large areal extent and constant thickness occurred. A further feature of these studies was that the penetrator material and its

geometry were also held constant in each experiment, and adequate control on pitch and yore gave confidence in the reproducibility of results.

Figure 4 shows the data for three thicknesses of five ceramics placed onto a steel semi-infinite witness block and laterally confined, and impacted with the same projectile. The curves show the depth of penetration recorded in ceramic and steel, converted (in the Fig. 4(b). to areal density, ρ_A, to mediate for the differing densities encountered between the different ceramics thus

$$\rho_A = \rho_c t + \rho_{4340} d, \tag{3}$$

where t represents the thickness of ceramic plate whose density is ρ_C, and d represents the penetration distance into 4340 (ρ_{4340}). There is an additional point where no ceramic plate was added to the block and impact was allowed to occur directly upon it showing response of a metal rod penetrating a metallic target.

In all experiments, residual penetration depth was measured into a block of 4340 steel with ceramic tiles of different target strengths bonded to the front. Each tile/backing laminate was impacted by a 25.4 mm long, 6.35 mm diameter (L/D 4) tungsten rod at 1750±50 m s^{-1} [20]. One point, at a penetration depth of 35.3 mm, was obtained by the rod impacting a monolith consisting just of the semi-infinite 4340 steel backing block. Figure 4(a). shows the correlation between penetration depth and strength. Clearly there is little obvious dependence discernible from this measure. Neither are there other correlations with properties of the as received material. However, Fig. 4(b). shows a clear correlation between failed strength and areal density. Considering that there is a spread of velocities, and that a range of processes operate in the flow around a projectile through a comminuted ceramic that are not reproduced in plate impact, the relation is strong. It is particularly noteworthy that the metal too follows the trend established by the ceramics. The points in red represent values for steel and alumina discussed above. It is interesting to note that the material with the highest HEL, B_4C, does not have the best performance as might be expected on the basis of purely its strength since beyond this elastic value its strength rapidly falls away relative to the other ceramics.

The results of Fig. 4(b). clearly show the correlation between the ballistic performance of the ceramic and inelastic strength of the alumina recorded. The assumptions of instantaneous collapse of a material onto an inelastic response curve can only be reconciled with performance if account is taken of the relaxation time for the mechanism under consideration as shown above [23].

Conclusions

Continuum measurements of strength histories near the impact face of metals and ceramics have shown that the strength decays from an elastic to an inelastic state with kinetics dependent upon operating mechanisms. In the case of BCC metals, high Peierls barriers to slip slows relaxation from an elastic to a plastic state in ca. 500 ns. In the case of glasses the material holds its elastic strength for a similar time before the strength starts to decay to its inelastic state by the interconnection of microcracks. The alumina AD995 has grains, within which slip systems are limited, and a brittle intergranular glass phase. It too shows itself capable of retaining its elastic strength for around 500 ns before relaxing to a failed state. After an integrated loading, shock and recovery of AD995 alumina has shown evidence of twinning in the grains above the lower elastic limit of the composite ceramic and trans- and intergranular fracture within the microstructure in this range.

The above indicates that in order to investigate these effects, a means of delivering impulses of idealized form to reach a range of amplitudes is required. Each process investigated must respond to a step rise for its relaxation time and reach a threshold for triggering before its effects can be observed. The impulse required to track and describe

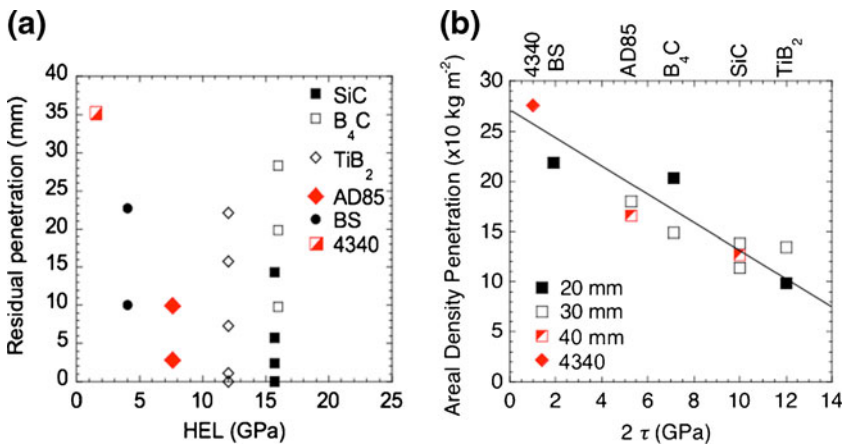

Fig. 4 (**a**) Residual penetration vs. HEL for the six materials. (**b**) Areal density vs. strength in the failed state for 4340 steel and armour ceramics subject to normal impact at 1750 m s^{-1}. Red points indicate the metal and alumina targets discussed earlier [21, 22]. Thicknesses refer to ceramic plates on 4340 semi-infinite backing

these mechanisms is the shock which must be maintained until the characteristic time for the process has been exceeded. The loading pulse applied in laboratory platforms ranges from fractions of a second to of order one nanosecond as the pulse amplitude rises. Thus the trade of amplitude and time duration must be set to match the deformation mechanism operational in the loading application to be described. In the case of long rod ballistic impact, impulse on the target surface preconditions material ahead of penetrating projectiles. Such impulses of microsecond duration are necessary to fail brittle solids.

Micromechanics control the conditioning of the impact zone ahead of an incoming penetrator and the density of nucleation sites and nature of fracture in the projectile's path and penetration depth into the ceramic scales with the failed strength of the materials independent of whether the targets are metals, brittle glasses or polycrystalline ceramics. From the onset of penetration to the end of the process the loading is under compression and this continues to the point at which the rod becomes stationary in a DoP experiment. The kinetics of damage and flow are thus set up in initial states and the times taken for compressive failure are of a different magnitude to those that occur in steady state penetration that occurs later. The correlation between the measurements of strength in the first microseconds and the results of DoP experiments where the target strength experienced by the rod in steady state penetration is less, indicates that the inelastic processes probed in plate impact govern failure in these targets.

Thus it is both the strength of strong ceramics, and the time required to fail them that controls conditions in the impact zone that defines the failure of the material. This is a function of the point at which they undergo inelastic flow. The inelastic state in this class of materials is by microfracture which is a function of the density of defects activated by plasticity mechanisms within the grains and in the amorphous intergranular phase. Future work must completely define the mechanisms by which materials operate when subject to load since understanding the kinetics at work within the materials in these states will allow better design of protective structures for civilian protection in the future.

Inhomogeneity is present in all natural systems and gives rise to defects at distinct scales within materials. These defects have a pivotal role in thermomechanical loading since they act as starting points for the onset of deformation within the microstructure. They are typical of the classes of material scale that they inhabit; the quantum, atomic, mesoscale, and continuum regimes defined in terms of the scales of the inhomogeneities that interact to drive the deformation mechanisms operating. As the applied impulse becomes longer, the material undergoes a larger number of operating mechanisms and the response observed at the end of process is the integrated suite of these, further, the duration of this pulse also filters the suite available to operate in compression since this state is relieved as expansion reaches sites within a target and components return to the elastic regime. It is the suite of mechanisms in compression that determines the state achieved and condition the target for penetration to incoming projectiles. These defects are activated further in tension for finite thickness targets and the performance will be worse in this case.

References

1. Gupta YM (1999) Mater Res Soc Symp Proc 538:139–150
2. Gupta YM (2000) In: Furnish MD et al. (ed) Shock Compression of Condensed Matter - 1999, 3–10
3. Rosenberg Z et al (1994) In: Brebbia CA (ed) Shock and Impact on Structures. Computational Mechanics Publications, Southampton, pp 73–105
4. Bourne NK, Millett JCF, Rosenberg Z, Murray NH (1998) J Mech Phys Solids 46:1887–1908
5. Bourne NK, Green WH, Dandekar DP (2006) Proc R Soc A 462 (2074):3197–3212
6. Kadau K, Germann TC, Lomdahl PS, Albers RC, Wark JS, Higginbotham A, Holian BL (2007) Shock waves in polycrystalline iron. Phys Rev Lett 96(13):135701
7. Bourne NK (2008) Int J Imp Engng 35:674–683
8. Rosenberg Z, Bless SJ, Brar NS (1990) Int J Impact Engng 9:45–49
9. Rosenberg Z, Yeshurun Y (1988) Int. J Impact Engng 7:357–362
10. Gray GT III, Bourne NK, Millett JCF (2003) J Appl Phys 94:6430–6436
11. Asay JR, Ao T, Vogler TJ, Davis J-P, Gray GT III (2009) J Appl Phys 106(7):073515
12. Bourne NK, Gray GT III, Millett JCF (2009) J Mat Sci, in press
13. Bourne NK, Millett JCF, Field JE (1999) Proc R Soc 455:1275–1282
14. Bourne NK, Rosenberg Z et al (1996) In: Schmidt SC (ed) Shock Compression of Condensed Matter 1995. American Institute of Physics, Woodbury, pp 567–572
15. Bourne NK, Rosenberg Z, Field JE (1995) J Appl Phys 78:3736–3739
16. Grady DE (1998) Shock wave compression of brittle solids. Mech Mater 29:181–203
17. Bourne NK, Millett JCF, Chen M, Dandekar DP, MacCauley JW (2007) J Appl Phys 102:073514
18. Chen MW, McCauley JW, Dandekar DP, Bourne NK (2006) Nature Materials 5(8):614–618
19. Alekseevskii VP (1966) Fizika Goreniya Vzryra 2:99
20. Tate A (1967) J Mech Phys Solids 15:387–399
21. Reaugh J, Holt A, Wilkins M, Cunningham B, Hord B, Kusubov A (1999) Int J Imp Eng 23:771–782
22. Rosenberg Z, Dekel E, Hohler V, Stilp AJ, Weber K (1998) In: Shock Compression of Condensed Matter 1997, 917–920; Woodbury, New York, American Institute of Physics
23. Bourne NK (2011) Mat Trans doi:10.1007/s11661-011-0720-1.